INVESTIGATION OF INERTIAL FACTORS INVOLVED IN AIRBAG-INDUCED FOREARM FRACTURES

Warren N. Hardy
Lawrence W. Schneider
University of Michigan Transportation Research Institute
United States
Paper Number 98-S7-O-13

ABSTRACT

Unembalmed, human cadavers were used in direct-contact, airbag-interaction deployments to assess the influence of upper-extremity inertia during vehicle deceleration on the likelihood and severity of airbag-induced forearm fractures. Comparisons were made for static and dynamic test configurations. Dynamic conditions were simulated by accelerating the steering-wheel/airbag module assembly toward the cadaver at the time of airbag deployment, with the cadaver forearm in contact with the airbag module. The results of the dynamic simulations suggest that the increased inertia of the upper extremity due to crash deceleration does not influence the incidence or severity of forearm fractures resulting from direct forearm airbag interaction. Also, the inertial loading of the airbag by the forearm did not significantly change the deployment characteristics of the airbag. The results of this study reinforce the efficacy of conducting static airbag deployments to assess airbag aggressivity and the potential for forearm fractures. The results also support the use of a simple kinematic measure, such as peak distal forearm speed (PDFS) or average distal forearm speed (ADFS), for the prediction of airbag-induced upper-extremity fractures.

INTRODUCTION

A number of recent research efforts have focused on airbag aggressivity assessment as well as upper-extremity fracture mechanisms and prediction. Saul et al. (1996) designed an instrumented Hybrid III arm for the assessment of direct-loading airbag-induced forearm fractures. The instrumented arm was used in six static deployments with three different airbag systems in two configurations to illustrate its ability to measure forearm bending moment, acceleration, and wrist velocity. The Research Arm Injury Device (RAID), a stylized surrogate upper extremity, was introduced and tested by Kuppa et al. (1997). Accident investigation data, inflator tank tests, and module characteristics were used to identify a set of driver airbags thought to be less or more injurious. The accelerations and bending moments measured by the RAID in a series of thirty-four static deployments using four different airbags were compared to the hypothesized relative aggressivity of the airbags. The performance of the RAID was compared to the performance of the instrumented Hybrid III by Johnston et al. (1997). Although the kinematics associated with each device were dramatically different, both the RAID and the instrumented dummy arm ranked the airbag systems similarly according to relative aggressivity.

Bass et al. (1997) examined a set of five driver airbags considered to range from less to more aggressive in a series of sixteen tests using human cadaver upper extremities excised at the proximal humerus. A load cell was fixed to the humerus with a universal joint simulating the shoulder. Two strain gage rosettes were applied to both the radius and ulna. Four additional tests were conducted using whole bodies. Four of the five airbags were also tested using the SAE fifth percentile female instrumented arm. The bending moments measured with the SAE arm were correlated with the observed fracture responses in the cadaver upper extremities. This indirect comparison suggested that 67 N-m represents a fifty-percent risk of ulna fracture and that 91 N-m represents a fifty-percent risk of both radius and ulna fracture.

Hardy et al. (1997) used seven unembalmed human cadavers to investigate upper-extremity injuries resulting from direct interaction with driver airbags. Seventeen static deployments were conducted using a steering-wheel-and-airbag assembly mounted to a fixed platform. Varying forearm-module proximity was investigated. Triaxial accelerometer mounts and crack detection gages were fixed to the bones of the forearm to measure general kinematics and fracture timing. The concept of using peak or average distal forearm speed (PDFS or ADFS) was introduced as a simple approach to the problem of predicting the potential for an airbag system to produce forearm fractures. Fracture is difficult to predict based upon the tolerance of bone to a given input because the tolerance of forearm bones varies along the length of the bones, and with the direction of the applied load relative to the cross section of the bones. However, fracture tolerance as indicated by bone mineral content, was found to be highly correlated with body and upper extremity mass. Distal forearm speed was also found to be related to upper extremity mass. The inter-relationship between tolerance, mass, and speed

produced a PDFS fracture threshold of 15.2 m/s, and an ADFS fracture threshold of 11.7 m/s. Proximity of the forearm to the airbag was found to greatly influence the incidence of fracture. It was stated that a simple airbag-aggressivity assessment tool could be based on measurement of distal forearm speed using static airbag deployments into a biofidelic, surrogate arm of appropriate mass.

Hardy et al. (1998) used four unembalmed human cadavers in eight direct-forearm airbag-interaction static deployments to assess the relative aggressivity of two different airbag modules. Instrumentation of the forearm bones included triaxial accelerometry, crack detection gages, and film targets. The forearm-fracture predictors, PDFS and ADFS, were evaluated and compared to the incidence of transverse, oblique, and wedge fractures of the radius and ulna. Internal-airbag pressure and axial column loads were also measured. The less-aggressive airbag system (LAS) produced half the number of forearm fracture as the more-aggressive system (MAS), yet exhibited a more aggressive internal-pressure performance. However, no direct relationship between internal-airbag pressure and forearm fracture was found. Both the peak internal pressure and the initial-inflation rate of the LAS were higher than for the MAS, but the PDFS, ADFS, and axial column loads of the LAS were lower. This inverse relationship between internal airbag pressure and airbag aggressivity prompted an investigation of the LAS and MAS design characteristics. It was hypothesized that the closed-module design of the LAS, coupled with longer, thicker tear seams, resulted in higher peak internal pressures and greater rates of pressure increase when compared to the MAS. Therefore, more inflator energy was used to achieve bag egress from the LAS module, making less energy available to be imparted to a forearm. The smaller and more distributed mass and size of the LAS doors may have assisted in the reduction of focused energy transfer to forearms, as would have the less-aggressive inflator of the LAS, as measured in tank tests. The results of this study supported the use of PDFS or ADFS for the prediction of airbag-induced upper-extremity fractures, and their application to airbag-aggressivity analysis.

Although preliminary methods for predicting forearm fractures and assessing relative airbag aggressivity have been developed, the influence of upper-extremity inertia on airbag deployment has not been previously investigated. Prior research has been limited to static airbag deployment scenarios. This study attempts to determine the effect that dynamic loading on the airbag by the upper extremity might have on fracture incidence and severity.

METHODS

Unembalmed, previously frozen human cadavers were used in direct-contact, airbag-interaction deployments to assess the influence of upper-extremity inertia on the likelihood and severity of forearm fracture and airbag aggressivity. Comparisons were made with each cadaver using static-column and dynamic-column test configurations. Instead of accelerating the cadavers toward the airbag, the airbag was accelerated toward the cadavers in the dynamic-column tests. One arm of each cadaver was subjected to a static-column deployment, while the other arm was tested using a stroking column. The static and dynamic configurations were alternated between left and right forearms from one cadaver to the next. In all tests, the middle of the pronated forearm was initially resting lightly on the center of the airbag module. The lower portion of the steering rim was modified to accommodate this configuration, while retaining the integrity of the rim. The airbag characteristics were consistent throughout the test series.

Static Tests

Static deployments were conducted with a steering-wheel-and-airbag assembly mounted to a fixed platform. Figure 1a and Figure 1b show a representative test configuration. The cadavers were placed in a supine position on the platform with the forearm positioned in the path of the deploying airbag. The cadaver was offset laterally from the center of the steering wheel, allowing free motion of the entire upper extremity. The upper extremity was positioned such that the forearm was perpendicular to the module tear seam with the middle of the pronated forearm near the center of the module. The hand was held loosely in place on the steering-wheel rim with perforated tape. The anterior forearm lightly contacted the airbag module in all tests. The angle of the elbow ranged between 170 and 180 degrees, and the steering wheel was inclined 30 degrees to vertical. After installation of the triaxial-accelerometer cluster and crack-detection-gage connections, the instrumentation cables were sutured to the shoulder and the forearm was wrapped lightly with utility tape. Thick padding was placed on the platform surface to eliminate the possibility of airbag-induced fling injuries.

Dynamic Tests

A Madymo model of a belt-restrained driver was used to determine the relative forearm-airbag module acceleration and velocity profiles necessary to conduct the dynamic-simulation cadaver tests in the laboratory. A 54-kph crash was simulated using a 30-G, 100-ms

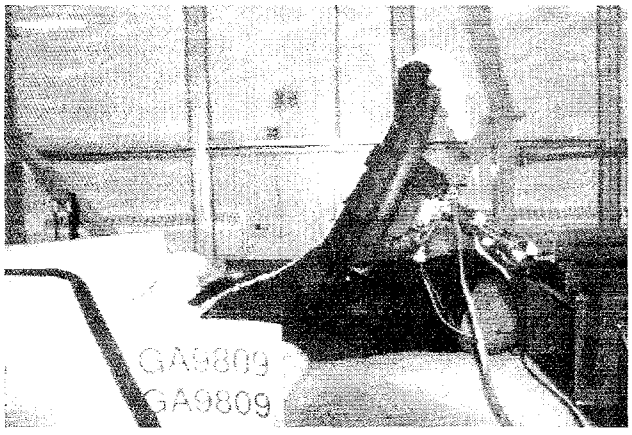

Figure 1a. A Lateral perspective of a typical static-deployment configuration.

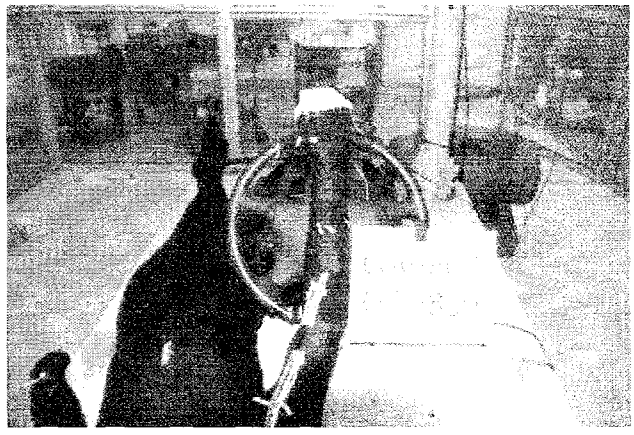

Figure 1b. A front view of the test shown in Figure 1a.

deceleration pulse. With the wrist positioned at the top of the steering rim and the middle of the forearm approximately 15.2 cm away from the center of the airbag module door, it was found that the peak relative speed between the forearm and airbag module was approximately 3 m/s after 30 ms, without the airbag firing but with the occupant belted. This suggested a 10-G acceleration of the forearm relative to (toward) the airbag just prior to deployment of the airbag.

Figure 2 shows the dynamic-simulation test fixture, which consists of a 25-cm stroke pneumatic cylinder, a guided square-tube ram, a load cell, and a steering-wheel/airbag-module assembly that is fixed to the ram. An adjustable support interfaces this fixture to the fixed platform. The stroke of the cylinder is snubbed by urethane padding placed between plates attached to the ram and the ram guide. The firing mechanism consists of a regulator, a 100-liter accumulator, a manual ball valve (safety valve), and a solenoid operated gate valve (fire valve). The cylinder inlet and outlets were enlarged to a 2.5-cm cross section and all associated piping is 2.5-cm inner diameter, to accommodate a 6-m/s stoke speed with and a 14-kg moving mass. The system operates using approximately 1.7 MPa (250 psi) nitrogen. Measured parameters include column forces and moments, column acceleration, column speed (inductive transducer), column displacement (laser transducer), triaxial distal forearm accelerations, and crack detection gage outputs (five forearm locations).

The cadaver and upper-extremity positions used for the dynamic simulations were the same as those used for the static deployments. The airbag was deployed approximately 30 ms into the stroke of the column, at which time the column had stroked between 5.0 and 7.5 cm, and the column speed was generally between 3 and 4 m/s. The total column stroke was limited to 15.2 cm with a peak speed of approximately 6 m/s after 50 ms. Thus, the column continued stroking throughout the airbag deployment. The ram, and therefore column, acceleration was essentially constant and the speed increased linearly prior to the deployment of the airbag. This was accomplished by controlling the motion of the cylinder up to the time of airbag deployment by ripping a metal plate, as shown in Figure 3. The ram was attached to this plate by a cable, and the opposite end of the plate was attached to a winch via a second cable. The winch was used to remove the slack from the cables prior to the test, and to adjust the length of the rip in the plate. This plate system provided approximately 5500 N (1250 lb) of constant resistance to the action of the cylinder, up to the time of airbag deployment. The pressure in the

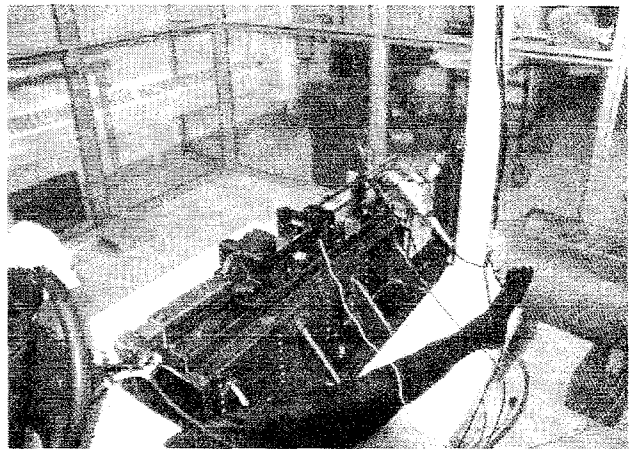

Figure 2. The dynamic-simulation test fixture for accelerating the steering-wheel/airbag-module assembly toward the cadaver forearm.

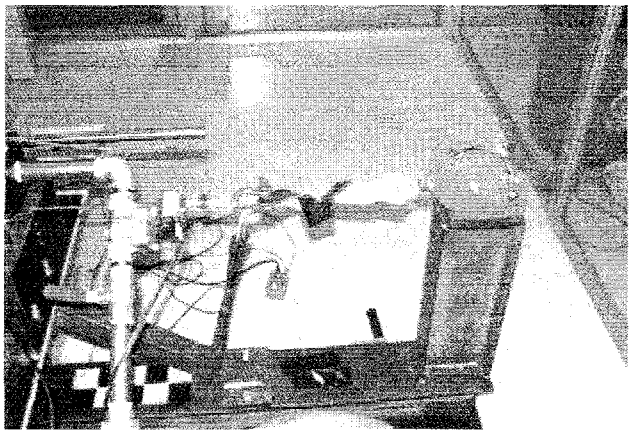

Figure 3. The ripping-plate mechanism used in the dynamic simulations to control the motion of the ram, prior to airbag deployment.

accumulator was set so that the cylinder was able to rip the plate and still provide roughly 10-G acceleration to the ram and column assemblies. The airbag was fired just as the plate ripped completely through, so that the extra force provided by the pneumatic cylinder upon ripping through the plate offset the reaction force of the airbag deployment and forearm interaction. This was done to minimize the effects of the forces developed during airbag deployment on the ram motion.

Figure 4a shows a ram acceleration trace, generated by averaging the ram accelerations obtained from five dynamic simulations. Five basic phases to the ram acceleration profile can be noted. The first phase of the trace corresponds to the start, overshoot, and settling of the ram. The second phase of the trace corresponds to ripping of the metal plate, which provides a nearly constant acceleration of approximately 10 G. Near the end of this phase the airbag is triggered, beginning the third phase at T=0 ms on the acceleration trace. During this phase there is a short period of deceleration, lasting about 1.5 ms. The fourth phase occurs after the deployment of the airbag. The column then accelerates at a higher rate, since its motion is no longer impeded by the deploying airbag or ripping plate. During the final phase, the motion of the column is arrested by urethane foam.

Figure 4b shows an averaged ram-velocity trace. The essentially constant nature of the column acceleration is evident here as the velocity ramps at nearly constant slope from -20 ms to +12 ms. There is only a slight disturbance during deployment of the airbag. Figure 4c shows an averaged ram-displacement trace.

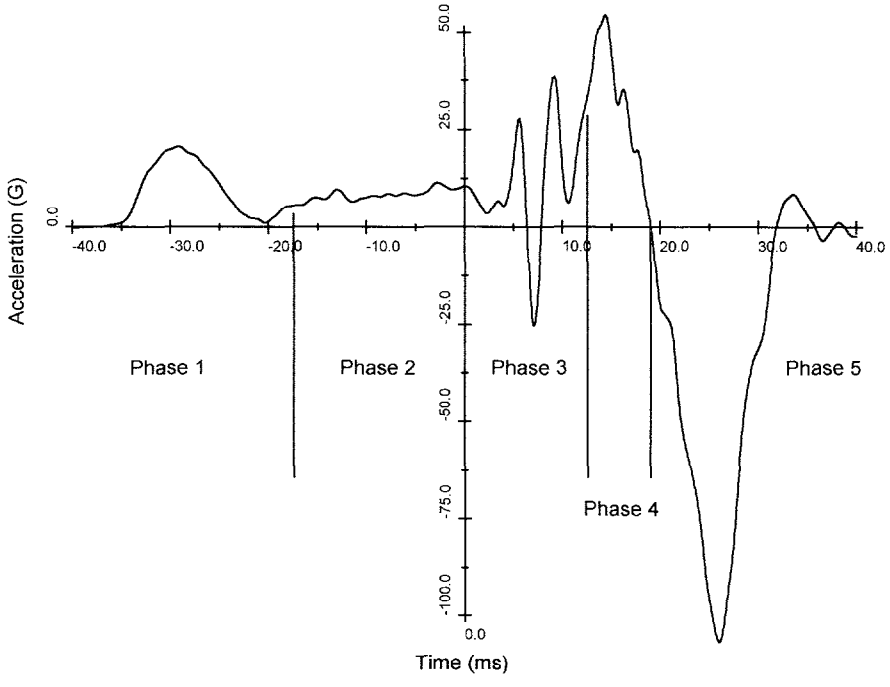

Figure 4a. Averaged dynamic-ram acceleration-time history (airbag triggered at T=0 ms).

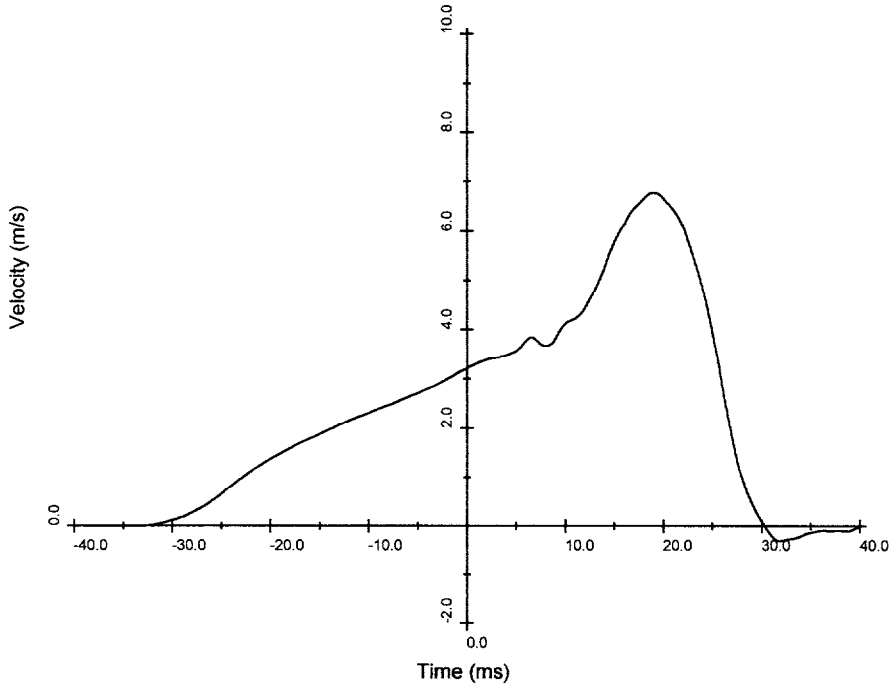

Figure 4b. Averaged dynamic-ram velocity-time history (airbag triggered at T=0 ms).

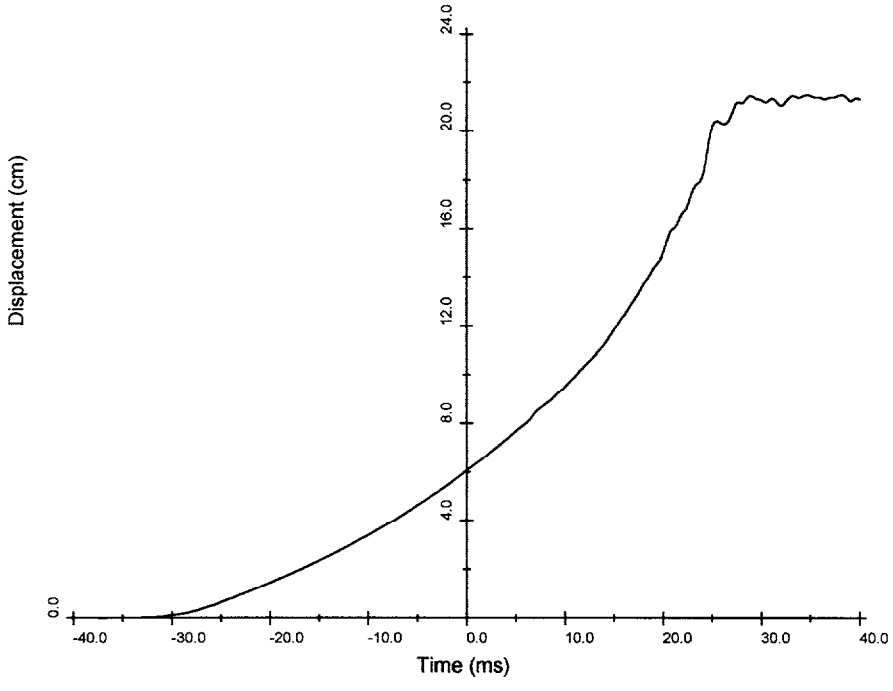

Figure 4c. Averaged dynamic-ram displacement-time history (airbag triggered at T=0 ms).

All signals were filtered using SAE Channel Class 300 Hz. These curves suggest that there was nearly constant loading of the airbag module by the forearm prior to and during the deployment. Any amount of energy transfer from the airbag to the driving mechanism was minor, and the overall energy of the system was greater than the static-deployment case.

Specimen Preparation

Figure 5 shows a typical forearm preparation prior to suturing of the wounds. Accelerometer mounting blocks made of Delrin were attached to the distal one-third region of the radius via plastic cable ties. Unlike previous tests, a target-mast block was not attached to the middiaphysis of the radius. Three crack detection gages were fixed to the radius in proximal, middiaphysis, and distal locations using cyanoacrylate. Two gages were also fixed to the middiaphysis and distal portions of the ulna. After instrumentation, pretest x-rays were taken of the forearms in pronation and supination.

Test Matrix

Ten deployments (G09 - G18) were conducted using five cadavers, three male and two female, as summarized in Table 1. Cadavers ranged in age from 65 to 85 years, with an average age of 76 years. The average stature and mass were 169 cm and 69 kg,

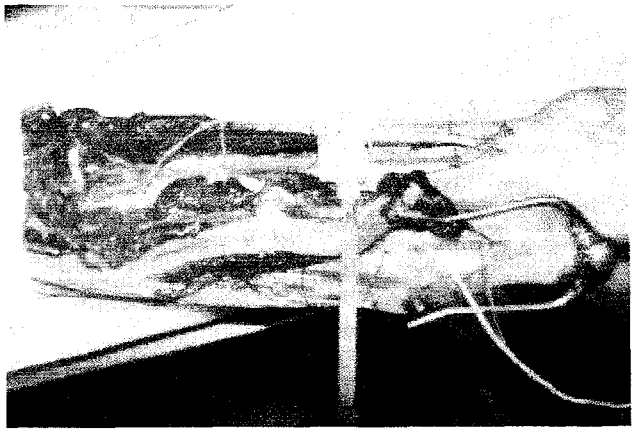

Figure 5. A typical forearm preparation after installation of the crack detection gages, prior to suturing.

respectively. One prototype airbag system was used for all tests. As previously noted, one static and one dynamic simulation deployment were conducted using each cadaver, so that direct comparisons could be made. The static and dynamic simulations were alternated between forearms, resulting in three dynamic and two static simulations on the right upper extremities, and two dynamic and three static simulations on the left upper extremities. The forearms and airbag modules were initially in direct contact and the steering column angle was 30 degrees to horizontal for all tests.

Table 1.
Matrix of Test Subjects and Conditions

Test	Gender	Age	Stature (cm)	Mass (kg)	Arm	Test Condition	Initial Spacing (cm)	Column Angle (deg)
G09	male	71	182	64	right	static	0.0	30
G10					left	dynamic	0.0	30
G11	male	74	181	77	left	static	0.0	30
G12					right	dynamic	0.0	30
G13	male	85	165	91	left	static	0.0	30
G14					right	dynamic	0.0	30
G15	female	65	164	61	right	static	0.0	30
G16					left	dynamic	0.0	30
G17	female	85	155	51	left	static	0.0	30
G18					right	dynamic	0.0	30
Avg.	-	76	169	69	-	-	0.0	30

After testing, posttest x-rays were taken, and the arms were disarticulated at the glenohumeral joint. At autopsy, forearm anthropometry was taken and the injuries were documented. The rate of mineralization and mineral content were determined by ashing 2 cm of the distal one-third of the radius and ulna. Peak and average distal forearm speeds were calculated and compared to fracture incidence and severity.

RESULTS

The test conditions and results are fully tabulated in Table A.1 of Appendix A. The observed injuries are cataloged in Appendix B.

Forearm-fracture timing was determined from the output of five crack detection gages that were installed on the bones of the forearms. Fractures of either the radius or ulna were found in nine of the ten tests, but one of these fractures was very minor. Missing fracture timing data resulted from gages not spanning a fracture or wires breaking during the test. All fractures captured by the crack detection gages occurred at the midulna position. However, this was not the only region that experienced fracture, nor were all of the fractures that occurred in this region captured by a crack detection gage. As discussed by Hardy et al. (1997), fractures coincide with local reductions in acceleration, and local speed plateaus, as shown in Figure 6 (Test G18). Figure 6 shows time histories of distal speed and resultant distal acceleration plotted with crack detection gage output. Time zero is defined as the point at which the airbag was triggered. The crack detection gage output, which indicates fracture, is the sharp vertical transition. This transition is associated with a commensurate drop in resultant distal acceleration, and a distal speed plateau.

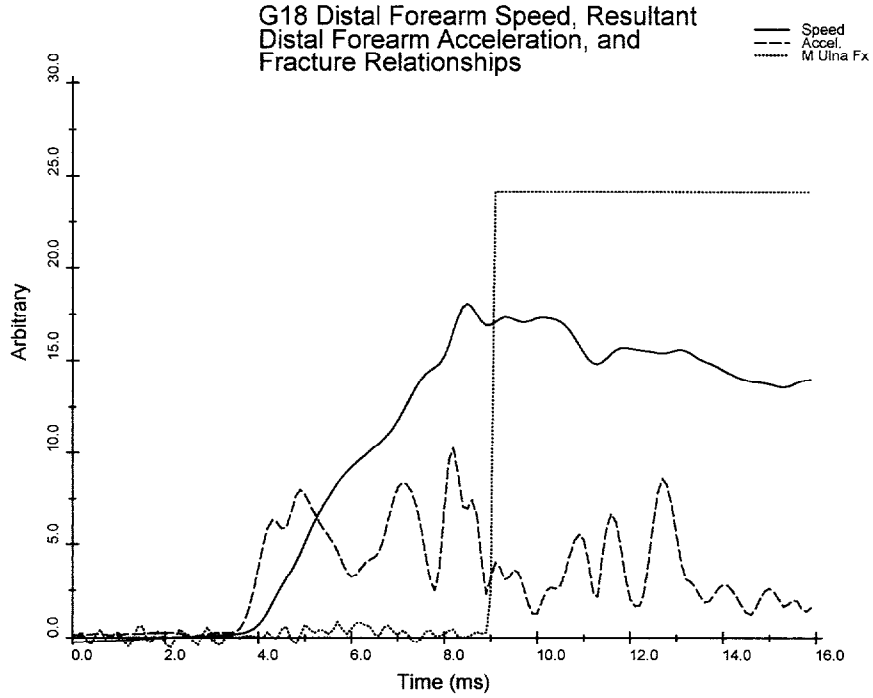

Figure 6. The relationship between distal forearm acceleration, speed, and fracture timing for G18.

The key results of the ten static/dynamic comparison tests are summarized in Table 2. Upper-extremity mass was measured after excising tissue in a circumferential fashion around the head of the humerus. Mineral content is expressed in grams of ash per centimeter of dry bone length. This is generally considered to be a more important parameter than rate of mineralization, since the quantity of bone available is as important as the quality of the bone, and mineral content reflects both quantity and quality of bone. The airbag-induced forearm-fracture predictors, peak distal forearm speed (PDFS) and average distal forearm speed (ADFS), were calculated over a 12-ms interval as described by Hardy et al. (1997), using the resultant magnitude of integrated triaxial accelerations. The 12-ms limit was selected to reduce the influence of integration errors and to minimize the effects of forearm rotations. The available crack-detection-gage information indicates that fractures occurred between 6 and 9 ms after triggering the airbag, supporting the use of a 12-ms interval. This information also shows that none of the measured fractures occurred within the short period of negative acceleration experienced by the stroking column. Each of the measured fractures occurred at a point during the column stroke when there was a substantial loading of the airbag by the forearm.

Table 2.
Summary of Test Results

Test	Gender	Arm	Extremity Mass (kg)	Mineral Content (g/cm) Ulna	Radius	Test Condition	Combined Distal Forearm Speed (m/s)	Peak Distal Forearm Speed (m/s)	Average Distal Forearm Speed (m/s)	Forearm Fractures	*Midulna* Fx Time (ms)
G09	m	r	3.22	0.61	0.78	static	-	-	-	2 ulna, 2 radius	-
G10		l	3.36	0.60	0.83	dynamic	19.5	14.0	11.7	2 ulna	-
G11	m	l	3.89	1.01	1.48	static	-	17.8	13.9	1 ulna (minor)	-
G12		r	3.94	1.25	1.43	dynamic	25.4	20.7	14.7	none	-
G13	m	l	4.40	0.87	1.04	static	-	18.2	14.8	2 ulna	6.9
G14		r	4.38	0.94	1.13	dynamic	22.0	18.4	12.4	2 ulna	8.6
G15	f	r	2.90	0.50	0.81	static	-	20.8	18.4	2 ulna	6.3
G16		l	2.77	0.69	0.80	dynamic	21.6	17.8	13.8	1 ulna	-
G17	f	l	1.95	0.43	0.55	static	-	-	-	1 ulna, 2 radius	6.2
G18		r	1.95	0.52	0.55	dynamic	20.6	17.7	14.4	1 ulna, 1 radius	9.0

In the dynamic-simulation tests, the distal forearm speed values result not only from the deploying airbag, but also from the velocity imparted by the stroking column. The combined distal forearm speed (CDFS) values include the contribution of the column. The PDFS values are obtained by subtracting the measured velocity time history of the column from the CDFS time history. The distal forearm speed curve shown in Figure 6 resulted from this procedure. Even though the forearm was in motion at the time the airbag was triggered at T=0 ms, the distal forearm speed does not increase from zero until T=4 ms. This method essentially removes the velocity contribution of the stroking column from the speed calculations, thereby isolating the effects of the airbag deployment from the stroking of the column. The ADFS values are calculated using this adjustment procedure as well.

Table 2 also summarizes the number of distinct ulna and radius fractures observed for each test. As indicated, both male and female specimens sustained fractures. These fractures can be divided into three general categories: simple, wedge, and complex, as suggested by Mueller et al. (1991). The observed injuries were largely transverse, oblique, and wedge fractures of the ulna or radius, or both, similar to those reported in field investigations. Tears of the elbow joint capsule were also found in some cases.

The most pronounced observation is the similarity between the static and dynamic-simulation results. The dynamic-simulation PDFS and ADFS values differ little from those obtained in the static tests. In one pair of tests, G13 and G14, the PDFS values differ by only 1 percent. The average PDFS and ADFS values for the dynamic simulations are 17.7 and 13.4 m/s, respectively, while the average PDFS and ADFS values for the static tests are 18.9 and 15.7 m/s, respectively. These slightly lower values obtained from the dynamic tests are reasonable because the accelerating forearm will appear heavier to the deploying airbag. The dynamic simulations produced essentially the same number and severity of forearm fractures as did the static tests. Examples of forearm fractures generated by static (right arm in Test G15) and dynamic (left arm, in Test G16) testing using a representative cadaver specimen are shown in Figure 7a and Figure 7b, respectively. Figure 7a (static) shows a transverse and a wedge fracture of the ulna, and Figure 7b (dynamic) shows a wedge fracture of the ulna. Both x-rays are of the supinated forearm.

The fracture thresholds for direct-contact conditions previously reported by Hardy et al. (1997) are summarized in Table 3. These values represent a fifty-percent probability of forearm fracture. All of the PDFS and ADFS values obtained from both the static and dynamic tests were above the threshold values, and forearm fractures were obtained in all tests except Test G12. While previous airbag/upper-extremity interaction tests have shown that some forearm bones are so weak that they would likely fracture under virtually any conditions, the forearm bones of the cadaver used for Test G12 represent the opposite extreme, having mineral contents of 1.25 and 1.43 g/cm for the ulna and radius, respectively. It is unlikely that these bones would fracture under even the most severe airbag-deployment conditions. The bones of the other forearm from this cadaver had similarly high mineral contents of 1.01 and 1.48 g/cm for the ulna and radius, respectively. The ulna from this forearm experienced a minor intra-articular fracture (chip) of the proximal ulna. In three tests, G10, G15, and G16, the mineral content of the radius was below the previously determined mineral-content threshold of 1.03 g/cm, yet the bones did not fracture. This suggests that a lower mineral-content threshold slightly lower than 1.03 g/cm may be more appropriate. All other fractures occurred in bones having mineral contents below 1.03 g/cm.

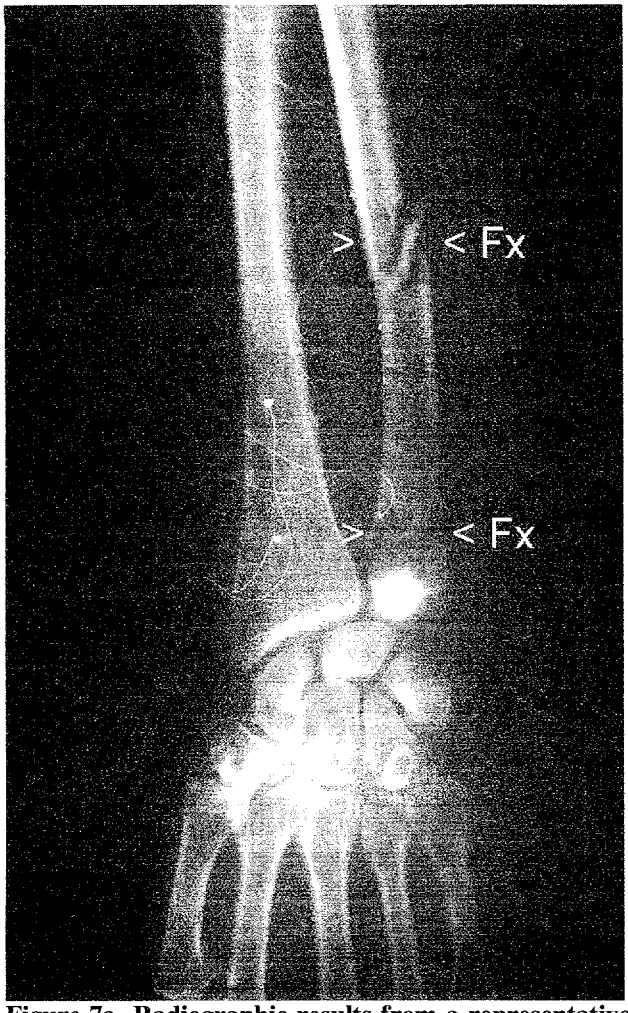

Figure 7a. Radiographic results from a representative static test (right arm, in supination).

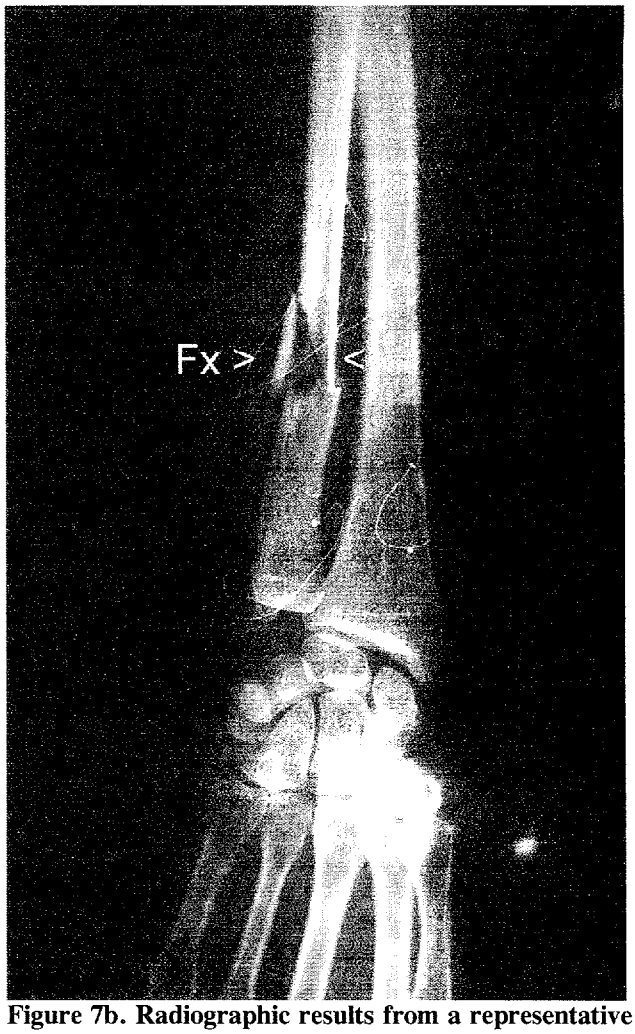

Figure 7b. Radiographic results from a representative dynamic simulation (left arm of the cadaver shown in Figure 7a, in supination).

Table 3
Prior Fracture Thresholds for Contact Conditions

Peak distal forearm speed (PDFS)	m/s	15.2
Average distal forearm speed (ADFS)	m/s	11.7
Upper extremity mass (UEM)	kg	2.9
Mineral content (MC)	g/cm	1.03

DISCUSSION

The results of these dynamic simulations suggest that increased inertia of the upper extremity, due to crash deceleration, does not influence the incidence or severity of forearm fractures resulting from direct forearm/airbag interaction. The results also support the use of a simple kinematic measure, such as PDFS or ADFS, for the prediction of airbag-induced upper-extremity fractures.

Within these tests, the inertial loading of the airbag by the forearm did not significantly change the deployment characteristics of the airbag. Although there was a 10-G preload applied to the airbag module by the forearm at the time of airbag deployment, and the airbag module was accelerated toward the forearm at approximately 50 G toward the end of the deployment (Phase 4 of Figure 4a), the deployment of the airbag was the overwhelmingly dominant effect on the response of the upper extremity. The peak distal forearm acceleration magnitudes ranged from approximately 700 to 1300 G in these tests. Given the large contribution of the deploying airbag and the low mass and small size of the typical upper extremity, the relatively small contribution of the simulated crash deceleration is apparently insignificant. Even with the forearm pressed against the airbag module prior to and during deployment, the forearm did not noticeably influence the

egress of the airbag from the module. These results suggest that the inertial effects of crash deceleration are of little concern to upper-extremity/airbag-interaction testing. This result differs from that encountered in other types of direct-interaction testing, such as out-of-position thorax/airbag-interaction tests, where the mass and size of the body significantly inhibit the egress of the airbag from the module. The dynamic simulation used in these tests differs from a real-world crash in that the entire cadaver was not subjected to the crash dynamics. However, given the flexible coupling of the forearm to the rest of the body through the elbow and shoulder, it is felt that this would have been a negligible effect.

While the accelerating airbag module had little effect on forearm fracture outcome, it had a dramatic effect on the distal forearm speed values. This is essentially due to the additive nature of the airbag module speed and the distal forearm speed for the initial phases of the airbag deployment. The airbag module speed curves, obtained using an inductive transducer, were subtracted from the distal forearm speed curves when calculating the PDFS values. This technique provides nearly the same result as simply subtracting the speed the airbag module had attained at the time the airbag was triggered. If the CDFS curves are tared using this approach, the resulting values differ from the PDFS values by an average 1.1 m/s. The combined distal forearm speed approximates the magnitude of the total change in velocity that would be experienced by a forearm during a dynamic crash event. During a dynamic crash event, the forearm first approaches the airbag prior to deployment, and then rapidly changes direction as the airbag deploys. In these dynamic simulations, the airbag module is first accelerated against the forearm, and then the airbag deploys. In this case, the motion of the forearm is in one direction, relative to the airbag module

As in previous static airbag deployment tests, the PDFS values were able to accurately predict forearm fracture except in one instance of an extremely high-tolerance forearm, indicating that there may be individuals whose forearm fracture tolerance is so great that these kinematic predictors are irrelevant.

The results of this study are significant because they reinforce the efficacy of conducting static airbag deployments in biomechanical investigations of airbag aggressivity with respect to forearm fractures. The majority of previous airbag/upper-extremity interaction testing has been performed using static deployments. The kinematics of static deployments are more repeatable and more easily defined. Also, static deployments are easier to conduct, and are far less costly than dynamic tests. This study provides additional support for the use of PDFS and ADFS in static deployment testing, and shows that static deployments are a meaningful method of evaluating upper-extremity/airbag-interaction parameters and fracture outcome.

In summary, these tests showed no appreciable difference in forearm fracture outcome between static deployments and dynamic simulations. Although the dynamic simulation method was not fully representative of the dynamics of a real-world crash, it is believed to have provided appropriate accelerations and energy to the cadaver upper extremity during crucial phases of the airbag deployment to substantiate this observation. In addition, the fracture predictors PDFS and ADFS performed well in this study.

CONCLUSIONS

The simple airbag-aggressivity and forearm-fracture predictors, PDFS and ADFS, have been used in a comparison of static airbag deployments and dynamic simulations. The results:

- support the use of PDFS or ADFS as predictors of airbag-induced forearm fractures;
- indicate that there is essentially no difference in fracture incidence or severity between static and dynamic conditions; and
- suggest static testing may be used to assess airbag aggressivity with respect to forearm fractures instead of more complicated and costly dynamic testing.

ACKNOWLEDGMENTS

This work was conducted by the University of Michigan Transportation Research Institute, Biosciences Division, and was carried out in accordance with the practices outlined by the Anatomical Donations Program of the University of Michigan Medical School.

Necropsy assistance and pathology analysis was provided by Dr. Kanu Virani, consulting forensic pathologist. The contributions of Anthony King, Thomas Jeffreys, and other UMTRI staff are greatly appreciated.

The work covered by this report was financed by GM pursuant to an agreement between GM and the U.S. Department of Transportation.

REFERENCES

Bass, CR; Duma, SM; Crandall, JR; Morris, R; Martin, P; Pilkey, WD; Hurwitz, S; Khaewpong, N; Eppinger, R; Sun, E (1997). The Interaction of Air Bags with Upper Extremities. *Proceedings of the 41st Stapp Car Crash Conference*, pp. 111-129. SAE, Warrendale, PA.

Hardy, WN; Schneider, LW; Reed, MP (1998). *Comparison of Airbag-Aggressivity Predictors in Relation to Forearm Fractures*. SAE Technical Paper No.980856. SAE, Warrendale, PA.

Hardy, WN; Schneider, LW; Reed, MP; Ricci, LL (1997). Biomechanical Investigation of Airbag-Induced Upper-Extremity Injuries. *Proceedings of the 41st Stapp Car Crash Conference*, pp. 131-149. SAE, Warrendale, PA.

Johnston, KL; Klinich, KD; Rhule, DA; Saul, RA (1997). *Assessing Arm Injury Potential from Deploying Air Bags*. SAE Technical Paper No. 970400. SAE Warrendale, PA.

Kuppa, SM; Olson, MB; Yeiser, CW; Taylor, LM (1997). *RAID - An Investigative Tool to Study Air Bag/Upper Extremity Interactions*. SAE Technical Paper No. 970399. SAE, Warrendale, PA.

Mueller, ME; Allgiower; M (1991). *Manual of Internal Fixation: Techniques Recommended by the AO ASIF Group*. Springer Verlag, New York, NY.

Saul, RA; Backaitis, SH; Beebe, MS (1996). Hybrid III Dummy Instrumentation and Assessment of Arm Injuries During Air Bag Deployment. *Proceedings of the 40th Stapp Car Crash Conference*, pp. 85-94. SAE, Warrendale, PA.

APPENDIX A Summary of Results

Table A.1
Summary of Specimen Attributes, Test Conditions, and Test Results

CADAVER	#	28889		28879		28838		28800		28942	
Gender	m/f	male		male		male		female		female	
Age	years	71		74		85		65		85	
Stature	cm	182		181		165		164		155	
Mass	kg	64		77		91		61		51	
Upper Extremity	r/l	r	l	l	r	l	r	r	l	l	r
Upper Extremity Mass	kg	3.22	3.36	3.89	3.94	4.40	4.38	2.90	2.77	1.95	1.95
Elbow to Finger Tip	cm	-	46	43	-	48	-	-	44	39	-
Elbow Circumference	cm	-	28	25	-	30	-	-	24	20	-
Mid-Forearm Circumference	cm	-	26	22	-	25	-	-	19	17	-
Wrist Circumference	cm	-	19	16	-	18	-	-	15	14	-
Biceps Circumference	cm	-	27	26	-	35	-	-	26	20	-
Humerus Circumference	cm	7.0	7.1	7.9	8.1	7.4	8.0	6.6	6.3	5.6	5.6
Length of Ulna	cm	29.0	29.0	27.3	28.0	26.5	27.6	25.5	25.3	24.0	26.0
AP Ulna Depth	cm	1.30	1.41	1.81	1.76	1.24	1.51	1.07	1.36	1.12	1.35
ML Ulna Width	cm	1.40	1.47	1.33	1.34	1.39	1.34	1.10	1.30	0.94	0.97
Ulna Rate of Mineralization	%	65.2	65.6	63.9	68.0	65.9	66.0	66.3	66.1	57.4	63.8
Ulna Mineral Content	g/cm	0.61	0.60	1.01	1.25	0.87	0.94	0.50	0.69	0.43	0.52
Length of Radius	cm	27.0	27.0	25.4	26.0	25.0	25.2	23.3	23.1	23.5	22.0
AP Radius Depth	cm	1.19	1.18	1.32	1.29	1.30	1.28	1.11	1.08	0.97	0.96
ML Radius Width	cm	1.76	1.61	1.95	2.01	1.55	1.57	1.25	1.26	1.18	1.16
Radius Rate of Mineralization	%	65.0	65.7	65.9	66.5	63.5	64.0	65.3	65.0	56.8	59.5
Radius Mineral Content	g/cm	0.78	0.83	1.48	1.43	1.04	1.13	0.81	0.80	0.55	0.55
TEST	#	G09	G10	G11	G12	G13	G14	G15	G16	G17	G18
Condition	sta/dyn	sta	dyn	sta	dyn	sta	dyn	sta	dyn	sta	dyn
Spacing	cm	0.0	0.0	0.0	0.0	0.0	0.0	0.0	0.0	0.0	0.0
Column Angle	deg	30	30	30	30	30	30	30	30	30	30
Fractures	#u,#r	2u,2r	2u	1u*	-	2u	2u	2u	1u	1u,2r	1u,1r
Capsular Tears	y/n	y	n	n	n	y	y	y	y	y	y
Combined Distal Forearm Speed	m/s	-	19.5	-	25.4	-	22.0	-	21.6	-	20.6
Peak Distal Forearm Speed	m/s	-	14.0	17.8	20.7	18.2	18.4	20.8	17.8	-	17.7
Average Distal Forearm Speed	m/s	-	11.7	13.9	14.7	14.8	12.4	18.4	13.8	-	14.4
Column Speed at Deployment	m/s	0.0	3.8	0.0	3.5	0.0	2.8	0.0	3.5	0.0	3.1
Peak Distal Acceleration Mag.	G	-	850	951	1032	709	779	899	1300	-	822
Time of Midulna Fx After Trigger	ms	-	-	-	-	6.9	8.6	6.3	-	6.2	9.0

* Very minor fracture

APPENDIX B Necropsy Results

The cadaver numbers are presented in the order of testing. The left and right arm information appears in the left and right columns respectively, regardless of the order of testing. Fracture locations are specified as the distance in mm from the distal end of the bone (styloid). Mineral contents (MC) are specified for both bones of the forearm.

Necropsy Results for Cadaver 28889

Male, 71, 64 kg, 182 cm

Left arm:	G10
Condition:	dynamic
Mass:	3.36 kg
Ulna MC:	0.60 g/cm
Radius MC:	0.83 g/cm

- Simple, oblique, distal fracture of the ulna starting anteriorly @ 20 mm, ending posterolaterally @ 42 mm
- Simple, oblique, diaphyseal fracture of the ulna starting anteriorly @ 41 mm, ending posterolaterally @ 68 mm, accompanied by a 27-mm chip

Right arm:	G09
Condition:	static
Mass:	3.22 kg
Ulna MC:	0.61 g/cm
Radius MC:	0.78 g/cm

- Single tear of the elbow joint capsule @ medial aspect of the ulna head (@ 7 mm)
- Simple, oblique, distal fracture of the ulna starting medially @ 23 mm, ending anterolaterally @ 41 mm
- Diaphyseal volar wedge fracture of the ulna starting anterolaterally @ 135 mm, centered medially @ 124 mm, ending laterally @ 185 mm
- Simple, transverse diaphyseal fracture of the radius @ 73 mm, accompanied by a 22-mm chip
- Simple, oblique, diaphyseal fracture of the radius starting laterally @ 185 mm, ending medially @ 194 mm

Necropsy Results for Cadaver 28879

Male, 74, 77 kg, 181 cm

Left arm:	G11
Condition:	static
Mass:	3.89 kg
Ulna MC:	1.01 g/cm
Radius MC:	1.48 g/cm

- Dislocation of the distal ulna
- Intra-articular 20-mm x 6-mm chip of the proximal ulna

Right arm:	G12
Condition:	dynamic
Mass:	3.94 kg
Ulna MC:	1.25 g/cm
Radius MC:	1.43 g/cm

- Negative

Necropsy Results for Cadaver 28838

Male, 85, 91 kg, 165 cm

Left arm:	G13
Condition:	static
Mass:	4.40 kg
Ulna MC:	0.87 gm/cm
Radius MC:	1.04 gm/cm

- Single tear of the elbow joint capsule @ anterior aspect of the radius head (@ 30 mm)
- Simple, oblique, diaphyseal fracture of the ulna starting anteriorly @ 62 mm, ending posterolaterally @ 48 mm
- Simple, oblique, diaphyseal fracture of the ulna starting anteriorly @ 165 mm, ending posterolaterally @ 184 mm

Right arm:	G14
Condition:	dynamic
Mass:	4.38 kg
Ulna MC:	0.94 g/cm
Radius MC:	1.13 g/cm

- Single tear of the elbow joint capsule @ anterior aspect of the radius head (@ 20 mm)
- Single tearing of the elbow joint capsule @ posterior aspect of the ulna head (@ 18 mm)
- Simple, transverse, diaphyseal fracture of the ulna @ 70 mm
- Simple, oblique, intra-articular fracture of the proximal ulna starting posteriorly @ 225 mm, ending anteromedially @ 242 mm

Necropsy Results for Cadaver 28800

Female, 65, 61 kg, 164 cm

Left arm: G16
Condition: dynamic
Mass: 2.77 kg
Ulna MC: 0.69 g/cm
Radius MC: 0.80 g/cm

- Single tear of the elbow joint capsule @ lateral aspect of the radius head (@ 25 mm)
- Diaphyseal anteromedial wedge fracture of the ulna starting anteriorly @ 44 mm, centered laterally @ 52 mm, ending anteromedially @ 65 mm

Right arm: G15
Condition: static
Mass: 2.90 kg
Ulna MC: 0.50 g/cm
Radius MC: 0.81 g/cm

- Single lateral tear of the elbow joint capsule @ lateral aspect of the radius head (@ 23 mm)
- Single vertical tear of the elbow joint capsule @ lateral aspect of the ulna head (@ 25 mm)
- Simple, transverse, distal fracture of the ulna @ 17 mm
- Diaphyseal anteromedial wedge fracture of the ulna starting anteriorly @ 64 mm, centered laterally @ 71 mm, ending anteromedially @ 84 mm

Necropsy Results for Cadaver 28942

Female, 85, 51 kg, 155 cm

Left arm: G17
Condition: static
Mass: 1.95 kg
Ulna MC: 0.43 g/cm
Radius MC: 0.55 g/cm

- Single oblique tear of the elbow joint capsule @ anterior aspect of the radius head (@ 27 mm)
- Single transverse tear of the elbow joint capsule @ lateral aspect of the radius head (@ 31 mm)
- Dual wedge fracture of the ulna starting anteromedially @ 61 mm, centered laterally @ 73 mm, ending anterolaterally @ 87 mm
- Simple, oblique, diaphyseal fracture of the radius starting laterally @ 134 mm, ending anteromedially @ 145 mm
- Dual wedge fracture of the radius starting anteromedially @ 67 mm, centered laterally @ 80 mm, ending anteriorly @ 87 mm

Right arm: G18
Condition: dynamic
Mass: 1.95 kg
Ulna MC: 0.52 g/cm
Radius MC: 0.55 g/cm

- Single transverse tear of the elbow joint capsule from the medial aspect of the ulna head to the lateral aspect of the radius head (@ 75 mm)
- Simple, transverse, diaphyseal fracture of the ulna @ 52 mm, accompanied by a 8-mm chip
- Simple, oblique, distal fracture of the radius starting medially @ 25 mm, progressing along the anterior surface to 38 mm, ending laterally @ 32 mm